This article has been accepted for publication in IEEE Transactions on Cognitive Communications and Networking. This is the author's version which has not been fully edited and content may change prior to final publication. Citation information: DOI 10.1109/TCCN.2025.3567608

A Comprehensive Analysis of Secondary Coexistence in a Real-World CBRS Deployment

Armed Tusha*, Seda Dogan-Tusha*, Joshua Roy Palathinkal*, Hossein Nasiri*, Muhammad Iqbal Rochman*, Patrick McGuire†, and Monisha Ghosh*
*Department of Electrical and Electronics Engineering, University of Notre Dame, South Bend, IN, USA
†South Bend Community School Corporation, South Bend, IN, USA
Email: {atusha, stusha, jpalathi, hnasiri2, mrochman, mghosh3}@nd.edu, pmcguire@southbendin.gov

***Abstract*—The Federal Communications Commission (FCC) in the U.S. has made the Citizens Broadband Radio Service (CBRS) band (3.55 - 3.7 GHz) available for commercial wireless usage under a shared approach, controlled by Spectrum Access System (SAS). This paper presents a first-of-its-kind extensive measurement campaign of a commercial CBRS network that quantifies both co-channel interference (CCI) and adjacent channel interference (ACI) caused by competing Generalized Authorized Access (GAA) devices and C-band 5G, respectively. We (i) identify a particular CCI scenario and improve performance by changing the frequency allocation based on our study of other allocations in the vicinity and (ii) quantify ACI from 5G in C-band using throughput. We investigate user-experienced propagation loss and compare it with calculated propagation loss using CBRS 1+ specified Irregular Terrain Model (ITM) and empirical signal propagation models. We conclude that (i) CCI and ACI for GAA users is not handled well by the SAS, (ii) proper frequency allocation for GAA requires additional analysis of interference from other GAA users followed by dynamical channel selection, (iii) utilization of immediate adjacent channels by high power 5G deployments limits the performance of CBRS, and (iv) CBRS 1+ specified ITM overpredicts propagation characteristics in non-line-of-sight (NLoS) area.**

***Index Terms*—CBRS, GAA, co-channel interference, adjacent channel interference, throughput.**

I. Introduction

A. Overview of CBRS Band

The demand for spectrum is growing rapidly with the advancement of wireless technologies that enable new services and applications [1]. In response to this increasing demand, future spectrum allocation schemes are expected to adopt a sharing strategy, particularly with bands currently assigned to federal services. In light of this, in April 2015, the U.S. Federal Communications Commission (FCC) authorized the Citizens Broadband Radio Services (CBRS) band, $3.55-3.7$ GHz, for shared use by commercial wireless providers, while protecting the incumbent federal user, primarily Navy radar. As shown in Fig. 1, CBRS users are grouped into three different tiers based on their spectrum access priorities [2]. Incumbent users are designated as Tier 1 [3] and must be kept interference-free from both Tier 2 and Tier 3, known as Priority Access License (PAL) and Generalized Authorized Access (GAA), respectively [4]. The transmit power of Tier 2 and Tier 3 users is capped at 30 dBm/10 MHz for indoor use and 47 dBm/10 MHz for outdoor use. Tier 2 (PAL) and Tier 3 (GAA) users are primarily commercial wireless service providers deploying public and private wireless networks using 4G, 5G and proprietary technologies [5].

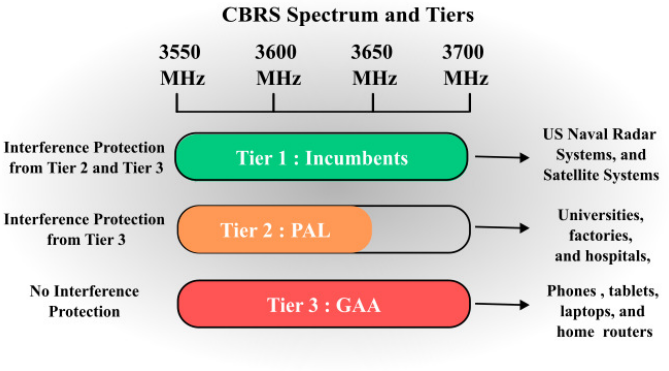

Fig. 1: Three-tier hierarchical architecture of CBRS band.

PAL operation is limited to the channels between $3550-3650$ MHz while GAA users have access to the entire 150 MHz band, but can access only those channels that are not being occupied by Tier 1 and Tier 2 users for a given frequency, time and area [6]. The Spectrum Access System (SAS) manages access for both PAL and GAA users, allowing them to transmit only after it assigns channels and ensures protection for higher-priority users. However, this is not a dynamic process, as the SAS conducts aggregate interference calculations each time channels are allocated to new users. As CBRS usage expands, this could become problematic, as the interference environment encountered by GAA devices can change rapidly, requiring swift adjustments in their operating frequencies.

Several companies have deployed private 4G Long Term Evolution (4G LTE) and 5G networks in public venues such as manufacturing plants, industrial internet-of-things, smart homes, stadiums, universities and other use cases, using CBRS [7] [8]. Mobile network operators such as Verizon also utilize the CBRS band in addition to their traditional licensed channels, using Carrier Aggregation (CA) and Dual Connectivity (DC), to increase the overall throughput. Competing GAA users in the same area thus experience co-channel interference (CCI) whether they are from the same deployment or from different deployments.

Furthermore, the $3.45-3.55$ GHz and $3.7-3.98$ GHz bands are immediately adjacent to CBRS and are allocated for exclusively licensed cellular networks [9], with permitted power spectral densities (PSDs) of 62 dBm/MHz for urban areas and 65 dBm/MHz for rural areas. These power levels are much higher than those of Citizens Broadband Radio Services Devices (CBSDs). C-band ($3.7-3.98$ GHz) services are being extensively deployed across various regions in the U.S. and 3.45 GHz services are in the early stages of deployment [10]. This leads to potential adjacent channel interference (ACI) from 3.45 GHz and C-band to CBSDs operating at the edges of the CBRS band. In [11], the authors performed detailed measurements and analyses of a real-world C-band deployment adjacent to an indoor CBRS deployment, where it was shown that the ACI level decreased by introducing a 20 MHz guard band between C-band and CBRS band.

Referring to the above discussion, propagation models can play a crucial role in better wireless network planning, CCI and ACI analysis, frequency assignment, and assessment of network parameters. These models are designed to predict the propagation loss of the signal strength received at a given distance and area, based on measurements from a mobile receiver [12]. In the initial release of the CBRS 1.0 standard, the Irregular Terrain Model (ITM) was applied as the propagation model for the CBRS band [13]. Later, with the release of CBRS 1+ specified ITM, additional propagation losses were introduced to enhance the original ITM. However, there is a notable lack of analysis based on real-world data for propagation loss calculations in the CBRS band, which could lead to critical improvements in the metrics reported back to the SAS for more effective spectrum management. This need for further analysis was highlighted in a recent FCC Notice of Proposed Rulemaking (NPRM) [14]. The study presented in this paper builds upon our previous work [15], where we focus on the analysis of secondary coexistence among GAA users in a real-world outdoor CBRS deployment that is exposed to CCI and ACI from its own network and an operator-deployed network in the C-band, respectively. In this extended version, we further shed light on the impact of propagation on network performance and potential propagation modeling for the CBRS spectrum.

B. Motivation & Main Contributions

Based on the above discussion, the main contributions of this paper are as follows:

- Extensive outdoor measurements of a commercial CBRS network in South Bend, IN, deployed by the local school district to provide affordable wireless broadband connectivity for students and their families in the area. The deployment consists of four base-stations (BSs), each with multiple CBSDs serving different sectors on different channels.
- Generating coverage heatmaps of throughput for each CBSD to evaluate the effect of different system parameters including height, frequency of operation, foliage and interference. In the absence of interference, we observed outdoor throughput of up to 140 Mbps. However, factors such as CCI, ACI, transmitter height, and foliage significantly reduced performance in many areas.
- We faced two interference scenarios in the deployment: (i) interference within the BS and between BSs due to frequency reuse by CBSDs, and (ii) interference caused by the utilization of both CBRS and C-band by Verizon in the same region at the same time. By studying frequency allocations and measuring signal strengths around the deployment, we proposed a new frequency allocation to mitigate CCI between two CBSDs. This adjustment resulted in an increase of $1-3$ dBm in Reference Signal Received Power (RSRP) and a $1-4$ dB increase in Reference Signal Received Quality (RSRQ), and consequently, usage of higher-order modulation and coding scheme (MCS), thereby demonstrating the importance of real-time interference-based frequency allocation.
- Compared to other CBRS channels, we observed a 12 Mbps of decrease in median downlink (DL) throughput for CBSDs operating on the 3690 MHz channel due to 5G deployments in the adjacent C-band channel ($3700-3760$ MHz) by Verizon.
- In addition to 5G in the C-band, Verizon BS also transmits on the CBRS band using LTE with CA (LTE-CA), aggregating up to five 20 MHz CBRS channels, and delivering a throughput performance that surpasses 5G throughput over C-band: this indicates that CBRS use by mobile operators will impact performance of smaller, private networks such as those deployed by the South

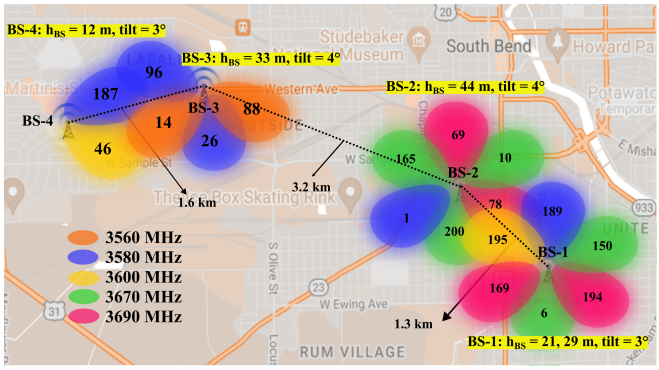

Fig. 2: CBRS deployment by the South Bend school district.

TABLE I: Height, PCI, and the center frequencies of the channel allocations for BSs.

Region	Height (m)	Channel Allocations (Center freq.)				
		3560 MHz	3580 MHz	3600 MHz	3670 MHz	3690 MHz
BS-1 (6 PCIs)	21 , 29		189	195	6, 150	169, 194
BS-2 (6 PCIs)	44		1		10, 200, 165	78, 69
BS-3 (4 PCIs)	33	14, 88	96, 26			
BS-4 (2 PCIs)	12		187	46		

TABLE II: Measurement tools and devices.

App./Tool	Features	Devices
SigCap	Operator, PCI, EARFCN, Band, Frequency, Altitude, Longitude, Latitude, RSRP, RSRQ, RSSI	1 × Google P5, 1 × Google P6, 1 × Samsung S21
QualiPoc	Operator, PCI, Band, Altitude, Longitude, Latitude, RSRP, RSRQ, CQI, RSSI, DL/UL Throughput, RB per subframe	2 × Samsung S22+
PRiSM	PCI, EARFCN, Frequency, Altitude, Longitude, Latitude, RSRP, RSRQ, RSSI	1 × Google P5

Bend school district.

- Since SAS does not offer information on 5G deployment in the adjacent upper or lower bands of the CBRS band, prior intelligence must be collected at the deployment site using measurement tools as those used in this study. This helps avoid interference and enhances link reliability and throughput, ultimately improving spectrum sharing from both network and user perspectives.
- Propagation analysis has been conducted to evaluate how well the CBRS 1+ specified ITM performs using real-world measurements. Additionally, comparisons have been made with other models specified by the 3rd Generation Partnership Project (3GPP), the International Telecommunication Union (ITU), and Winner II. The results indicate that while the CBRS 1+ specified ITM performs well in Line-of-Sight (LoS) areas, it struggles in Non-Line-of-Sight (NLoS) environments, underscoring the need for more accurate prediction methods for propagation loss in the CBRS spectrum.

II. DEPLOYMENT, TOOLS & METHODOLOGY

A. Deployment

An extensive measurement campaign was conducted over a wide area of approximately 12 km^2 where the South Bend school district has deployed CBRS, as shown in Fig. 2. Four BSs, i.e., James Whitcomb Riley High School (BS-1), Hayes Tower (BS-2), West Tower (BS-3), and Navarre Middle School (BS-4) have been deployed on school buildings and towers, enabling South Bend schools to launch its own private LTE network to serve students and families. To sustain high throughput and enhance system capacity, each BS has multiple CBSDs, each operating on a separate sectors at a maximum permitted EIRP of 47 dBm/10 MHz. Each CBSD is identified by its Physical Channel Identity (PCI) and operates over a single 20 MHz wide channel. Table I provides the details regarding these BSs, including their height, PCI, and the center frequencies of the channel allocations. Since there are only 7 non-overlapping 20 MHz channels in the CBRS band and the deployment has 18 PCIs, it is clear that CBSDs will reuse channels. Thus, channel reuse is introduced at each BS via sectorization at the expense of potential CCI. It should be noted that Google SAS shows that all 15 channels (10 MHz each) are available for GAA use in this deployment.

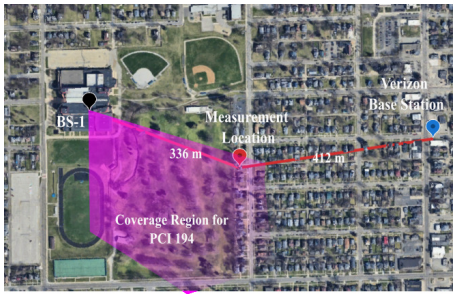

(a) The distance of measurement location from the BS-1 and nearby Verizon BS.

(b) Measurement setup.

Fig. 3: Measurement environment and setup for MC-3.

BS-1 is deployed on the roof of James Whitcomb Riley High School at a height of 29 m for PCIs 189 and 195, while the remaining PCIs are deployed at a height of 21 m. It uses four 20 MHz channels and six sectors with its corresponding PCIs listed in Table I.

BS-2 is mounted on a tower with a height of 44 m, and uses three channels across six PCIs, three of which operates on the same frequency (3670 MHz). The distance between BS-1 and BS-2 is about 1.3 km.

BS-3 is located on a tower at a lower height of 33 m when compared to BS-2, and it utilizes two channels, i.e., 3560 MHz and 3580 MHz to serve four sectors with PCIs as shown in Table I.

BS-4 is placed on the roof of Navarre Middle School at the lowest height of 13 m, and utilizes 3580 MHz and 3600 MHz channels to serve PCIs 187 and 46, respectively. The PCI 187 sector in BS-4 is directed towards PCI 96 and PCI 26 sectors in BS-3, which are operating on the same channel, thereby presenting a potential CCI scenario.

B. Measurement Tools

Smartphones were used as user equipments (UEs) to capture detailed signal information, using tools such as SigCap, QualiPoc, and PRiSM as shown in Table II.

SigCap is an Android application which collects wireless signal parameters (cellular and Wi-Fi) by using Application Programming Interfaces (APIs) without requiring root access [16]. It allows extraction of detailed signal parameters such as Received Signal Strength Indicator (RSSI), RSRP,

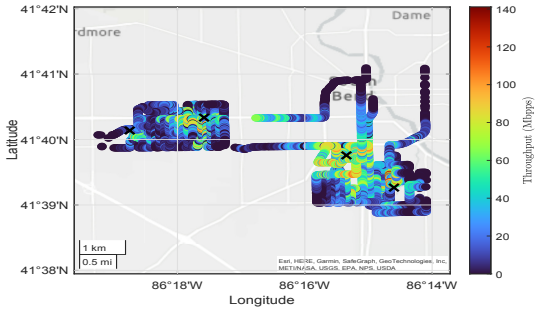

(a) Throughput performance.

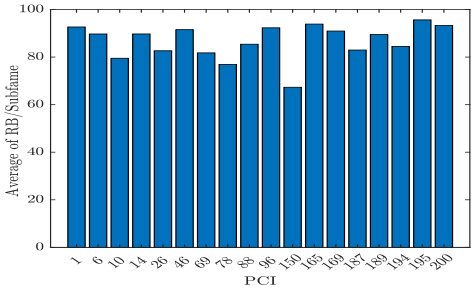

(b) Average RBs/subframe per PCI.

Fig. 4: Throughput performance and average RBs/subframe for each BS.

RSRQ, channel band and frequency for 4G, 5G, and Wi-Fi technologies every 5 seconds, along with location and time-stamps from the GPS receiver on the device.

QualiPoc is a commercial measurement application developed by Rohde & Schwarz and installed on Android phones [17]. In addition to signal parameters extracted by SigCap, QualiPoc collects MCS, block error rate (BLER), time division duplexing (TDD) configuration, channel quality indicator (CQI), and physical layer throughput. All downlink (DL) throughput results discussed in this work are extracted from QualiPoc, running an iperf utility.

PRiSM is a software-defined radio (SDR) based handheld network scanner for surveying 4G/5G networks and also operates as a spectrum analyzer from 70 MHz to 6 GHz [18]. It easily connects to PCs, tablets, and smartphones to monitor the frequency of interest. Unlike the above two tools, PRiSM does not require a SIM card to extract network information and uses the smartphone merely as a display and recording device to track channel occupancy.

C. Measurement Campaigns (MCs)

Driving and stationary measurements campaigns (MCs) were conducted during the summer months of 2023, when dense foliage covered the trees. The UEs connected to the CBRS network using SIM cards provided by the school district. Measurements of the Verizon network were collected using a 5G SIM with an unlimited data plan to avoid throttling. We grouped our experiments into three separate campaigns.

1) MC-1: Driving measurements were conducted around all CBSDs as shown in Fig. 4(a), at an average speed of 32 km/hour, over a time period of nearly 3 hours per CBSD.

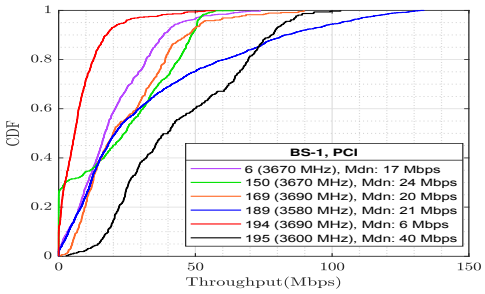

(a)

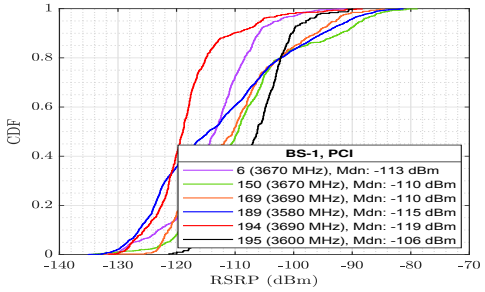

(b)

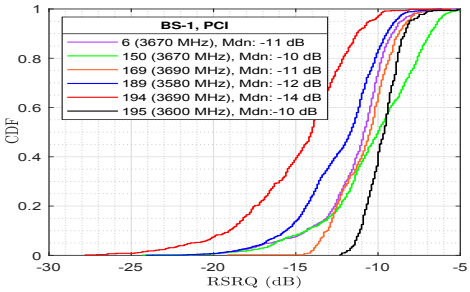

(c)

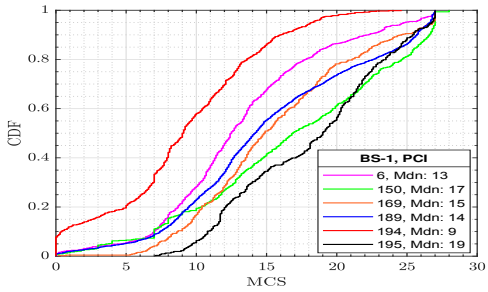

(d)

Fig. 5: CDF plots of throughput, RSRP, RSRQ and MCS for PCIs at BS-1.

QualiPoc, SigCap and PRiSM were used to collect data, running on the smartphones shown in Table II. DL throughput measurements were recorded on two Samsung S22+ phones with QualiPoc, while the PRiSM was connected to a Google Pixel5 (P5) and scanned all CBRS and C-band channels in order to identify other users operating in these bands.

2) MC-2: This campaign focused on BS-3 and BS-4, which are 1.6 km apart, to evaluate potential CCI in the deployment due to reuse of 3580 MHz frequency by CBSDs in these two

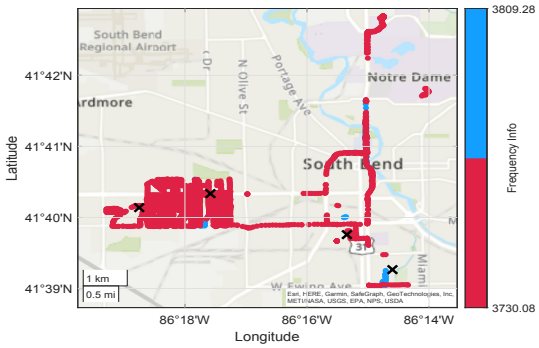

Fig. 6: The usage of C-band by Verizon in the region.

BSs. After identifying CCI, we collaborated with the network provider to adjust frequency assignments and evaluated the improvements after CCI was mitigated.

3) MC-3: To evaluate ACI caused by the C-band, we conducted focused, stationary, measurements between PCI 194 deployed on 3690 MHz in BS-1 and a nearby Verizon BS operating in $3700-3760$ MHz, as in Fig. 3. Fig. 3(a) shows the measurement location for MC-3, and its distance from BS-1 and the Verizon BS. The experiments were conducted in three phases to assess the performance of PCI 194 on 3690 MHz under ACI caused by the usage of C-band. CBRS and C-band users first conducted DL transmissions at different time instants, avoiding ACI. Then, they performed simultaneous DL transmissions, leading to ACI on CBRS band. After identifying ACI, we worked closely with the network provider to modify frequency assignments and assessed the improvements following the mitigation of ACI. Fig. 3(b) shows the devices used during MC-3. PRiSM was used to continuously monitor CBRS (Band 48) and C-band (n77/n78) usage.

III. Performance Results and Discussions

In this section, we present statistical analyses of the measurements under different conditions. The discussion is divided into four main categories: i) the performance of a real-world CBRS deployment, ii) CCI amongst GAA users, iii) ACI from C-band to CBRS, and iv) utilization of CBRS band by mobile operators and comparison with C-band.

A. Performance Evaluation

Fig. 4(a) illustrates the heat map of outdoor throughput obtained via driving measurements and Fig. 4(b) shows the distribution of resource blocks (RBs) per subframe across all PCIs in the deployment. The outdoor throughput observed is in the range of $20-40$ Mbps on average. The highest and lowest throughput was observed around BS-2 and BS-4, due to the heights of these BSs at 44 m and 12 m, respectively. The throughput around BS-2 is significantly higher compared to other BSs, primarily due to its elevated antenna placement and the relatively obstruction-free environment. In contrast, the low tower height of BS-4 results in a smaller area with high throughput. BS-1 is at a height comparable to BS-2; however, its coverage area is significantly smaller due to dense tree coverage, particularly to the southeast. Since throughput is

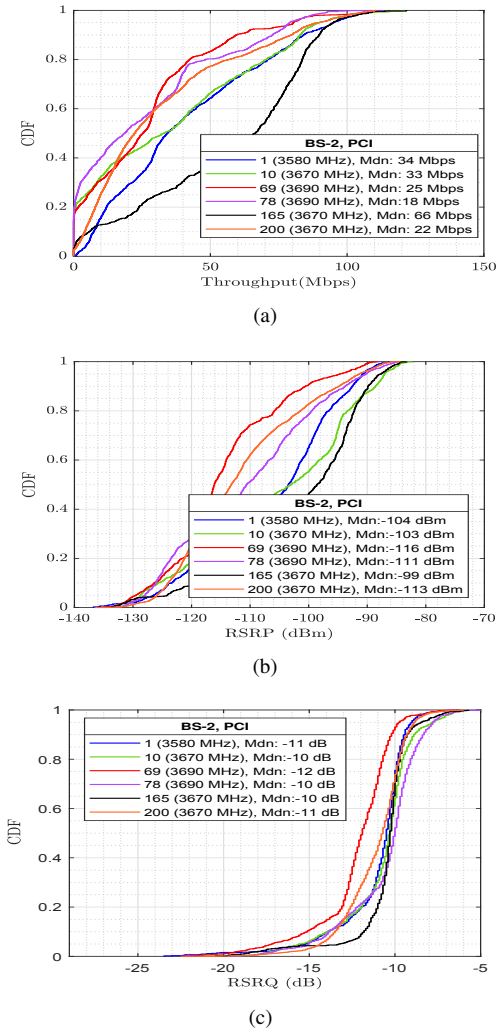

Fig. 7: CDF plots of throughput, RSRP and RSRQ for PCIs at BS-2.

primarily a function of the number of RBs allocated and MCS, we verify that the differences in measured throughput are not primarily due to RB allocation: Fig. 4(b) shows that the RB usage is approximately similar, with some differences that will be addressed later.

We analyzed the measured throughput, RSRP, and RSRQ for each BS using their cumulative distribution function (CDF) plots.

Performance of BS-1: Fig. 5 presents the results for each PCI of BS-1. PCI 195 has the best throughput in Fig. 5(a), nearly double that of the other PCIs, as it is the only PCI from BS-1 or BS-2 operating on 3600 MHz, as seen from Table I. This allows it to avoid CCI from other PCIs on the same channel. Similarly, the RSRP and RSRQ for PCI 195 outperforms the other PCIs in BS-1 as given in Figs. 5(b) and 5(c), respectively. PCIs 6 and 150 operate on 3670 MHz, while PCIs 169 and 194 operate on 3690 MHz. Although PCIs 6 and 150 showed similar median throughput performances at 17 Mbps and 24 Mbps, respectively, there is a substantial performance gap between PCI 169 and PCI 194, achieving 20

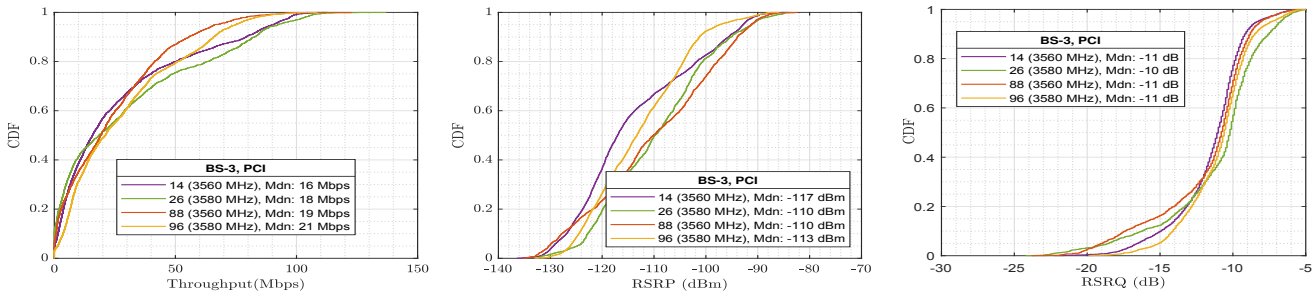

(a) (b) (c)

Fig. 8: CDF plots of throughput, RSRP and RSRQ for PCIs at BS-3.

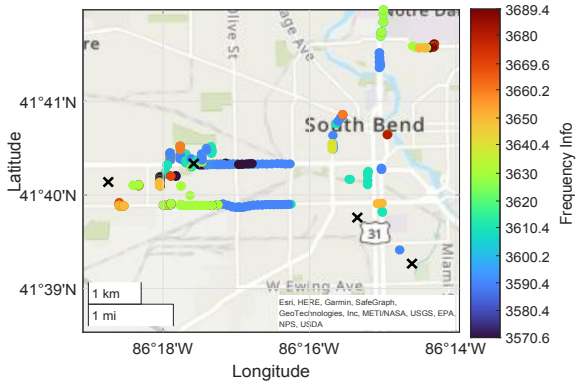

Fig. 9: CBRS band usage by Verizon in the region.

Mbps and 6 Mbps, respectively. PCI 194 also exhibited the worst RSRP, RSRQ and MCS performance as compared to the best performing PCI 195 in BS-1 as seen from 5(d), which explains the lower throughput. Based on our detailed analysis of signal strength measurements in the vicinity of BS-1, the reason for this is that PCI-194 experiences ACI due to the use of the immediately adjacent C-band, by a nearby Verizon BS, as shown in Figs. 3(a) and 6. The performance of PCI 194, both with and without C-band usage, will be discussed in Section III.C below.

Performance of BS-2: Fig. 7 shows the performance of BS-2, operating at a higher height than BS-1, and within an area where LoS propagation is more prevalent. Hence, PCI 165 on 3670 MHz achieves the highest median throughput of the CBRS deployment, reaching 66 Mbps as indicated in Fig. 7(a). The median throughput of PCI 165 is nearly double that observed on the other PCIs on 3670 MHz in BS-2 and BS-1, as PCI 165 is the only one directed northwest, while the rest are oriented southeast, potentially leading to CCI among them. PCI 200 has the lowest median throughput, 22 Mbps, amongst the PCIs on 3670 MHz in BS-2 due to its orientation toward a residential area with dense trees. As discussed for PCI 194 in BS-1, we observe that PCIs 69 and 78 on 3690 MHz have the worst performance in BS-2: this can be explained by ACI resulting from the usage of 3730 MHz in the vicinity of BS-2, as shown in Fig. 6. PCI 78 has the lowest median throughput of 18 Mbps on BS-2, and 7 Mbps lower than PCI 69, since its coverage overlaps with PCI 169 on 3690 MHz coming from BS-1, as seen in Fig. 2. RSRP results in Fig. 7(b) clearly exhibit the reduced impact of foliage on BS-2, where three PCIs (165, 1 and 10) have a median greater than -105 dBm. Similarly, in Fig. 7(c), the median RSRQ levels in BS-2 ranged from -12 dB to -10 dB, and provided better performance than BS-1. As in the throughput results, PCI 69 on 3690 MHz offered the lowest RSRQ performance due to the ACI.

Performance of BS-3: Fig. 8 presents the results of BS-3, which is less likely to suffer from interference since the distance of 3.2 km between BS-3 and BS-2 mitigates the presence of CCI, while the utilization of the lower edge of the CBRS band (3560 MHz and 3580 MHz) offers a sufficient guard band to avoid the effect of C-band ACI. Hence, all PCIs on BS-3 exhibit similar throughput, RSRP and RSRQ behavior, as shown in Fig. 8(a), Fig. 8(b) and Fig. 8(c), respectively. The obtained throughput levels at BS-3, including the peak throughput on PCI 88 (3560 MHz), is much lower compared to BS-2 due to lower tower height.

As shown in Fig. 2, BS-3's PCI 96 faces west. Given the short distance of 1.6 km between BS-3 and BS-4, coupled with the lower tower height of BS-3, this poses a potential CCI threat to PCI 187 in BS-4, which operates on the same frequency.

B. Avoiding CCI by selecting an appropriate frequency

MC-2 on PCI 187 evaluated the impact of CCI within the CBRS deployment itself and aims to improve system performance via a suitable frequency allocation.

Performance of BS-4: PCI 187 from BS-4, operating on 3580 MHz (S1) shows the worst throughput, RSRP and RSRQ, primarily due to CCI from PCI 96 of BS-3, as shown in Fig. 10. In contrast, PCI 46 from the same BS does not experience CCI and exhibits nearly the same performance as the PCIs on BS-3 as it is the only PCI operating on 3600 MHz in the region of BS-3 and BS-4.

To mitigate the impact of CCI on PCI 187, we proposed a frequency change from 3580 MHz (S1) to 3650 MHz (S2) based on our analysis of frequency allocations and signal strengths measurements in the vicinity of the CBRS deployment. The 3650 MHz channel was not being utilized by any of the BSs deployed by the school district, as seen from Table I. As illustrated in Fig. 9, Verizon has utilized the 3650 MHz

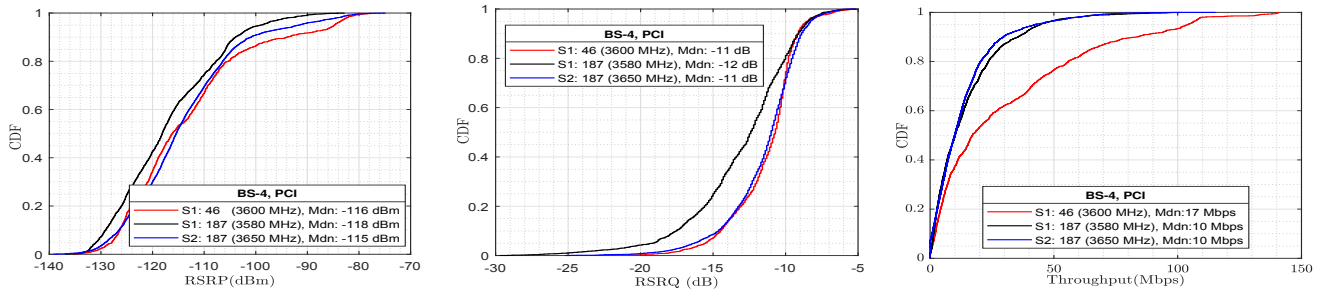

(a) (b) (c)

Fig. 10: CDF plots of RSRP, RSRQ, and throughput for BS-4 i) Scenario 1 (S1): PCI 187 on 3580 MHz and PCI 46 on 3600 MHz, and ii) Scenario 2 (S2): PCI 187 on 3650 MHz.

channel in the region of BSs, but not in the direction of PCI 187.

Fig. 10(a) and Fig. 10(b) show that changing the frequency of PCI 187 to 3650 MHz resulted in improved RSRP and RSRQ levels compared to the original frequency of 3580 MHz, bringing its performance closer to that of PCI 46, which is free from CCI. It is important to highlight that PCI 46 maintained the same performance after the frequency change on PCI 187, as they do not operate on the same frequency.

Compared to S1, the peak throughput of S2 increased by approximately 20 Mbps, from 100 Mbps to 120 Mbps, while the median throughput remained the same as shown in Fig. 10(c). This can be explained as follows: throughput is determined by the MCS and number of RBs allocated per subframe, as shown in Fig. 11. In Fig. 11(a), the median value of MCS for S2 increased by 2 indicating that 3650 MHz is exposed to less CCI compared to 3580 MHz, and the number of RBs also improved slightly, but not enough to deliver a significant throughput increase. We observe that PCI 46, for example, consistently achieves higher throughput due to a greater number of RBs/subframe, as shown in Fig. 11(b). It is speculated that the number of RBs/subframe allocated to PCI 187 was lower than that of PCI 46, likely due to proprietary network optimization algorithms. As a result, even though signal metrics such as RSRP, RSRQ, and MCS improved following the frequency change, the median throughput for PCI 187 remained unchanged, although the maximum throughput did increase.

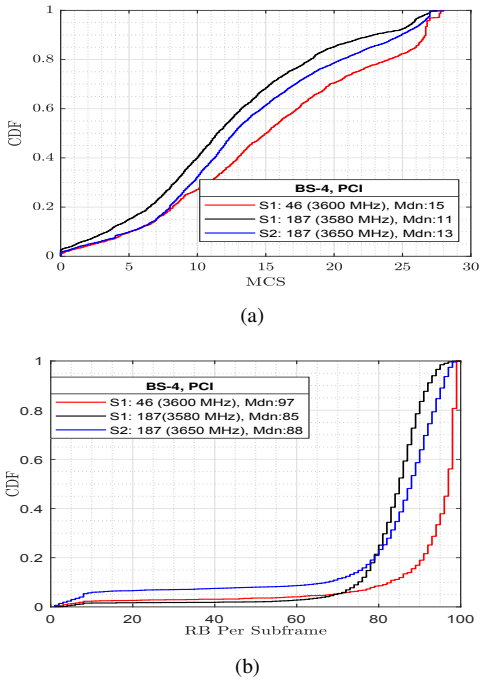

(a) (b)

Fig. 11: MCS and RBs per subframe for PCIs at BS-4.

C. Impact of ACI from C-band on CBRS

MC-3 on PCI 194 evaluates the impact of ACI caused by C-band on CBRS. We performed stationary measurements at the location indicated in Fig. 3(a), where the strongest RSRP was recorded for PCI 194 on 3690 MHz.

Fig. 12 illustrates the DL throughput performance when connected to PCI 194 in BS-1, both in the absence and presence of a Verizon C-band UE. First, we measured the DL throughput on the UE connected solely to the CBRS network, followed by simultaneous DL transmissions to two UEs – one connected to the CBRS network and the other connected to the C-band network. We observed approximately a 16% throughput degradation on the CBRS UE due to ACI from the C-band, when both devices were simultaneously connected. The CBRS UE achieved a peak throughput of around 80 Mbps when there was no transmission from the C-band UE. However, its maximum throughput dropped to about 60 Mbps in the presence of the C-band UE. Factors contributing to the reduced throughput on the CBRS UE include the absence of guard bands between CBRS and C-band, the difference in transmit power, and the lower tower height of BS-1 compared to the Verizon C-band tower.

Fig. 13 assesses the performance improvement of PCI 194 after a frequency change from 3690 MHz (S3) to 3560 MHz (S4). This change was made in response to our measurements that indicated significant ACI from C-band deployments to the network of South Bend school district operating at frequency 3690 MHz (S3). We conducted a driving measurement campaign in the PCI 194 coverage area with a new frequency 3560 MHz (S4) to assess the impact of proper frequency

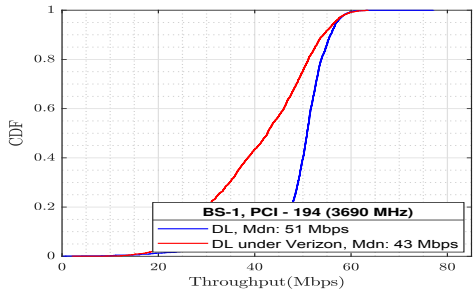

Fig. 12: The impact of C-band on PCI 194 (3690 MHz) at BS-1.

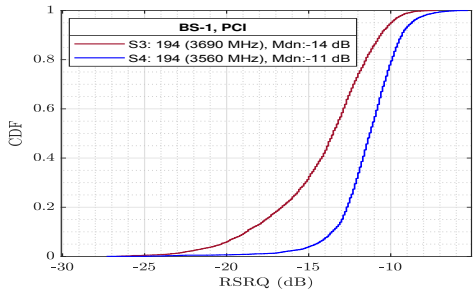

(a)

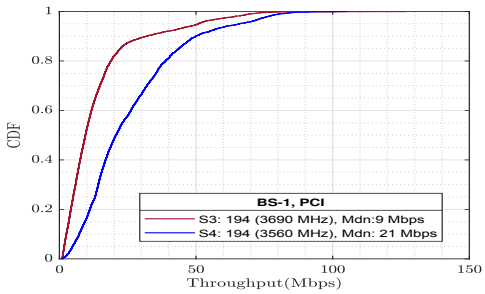

(b)

Fig. 13: RSRQ and throughput for PCI 194 i) Scenario 3 (S3): 3690 MHz, and ii) Scenario 4 (S4): 3560 MHz.

allocations on mitigating ACI from the C-band in the CBRS band. Fig. 13(a) shows that the change to S4 (frequency 3560 MHz) resulted in improved median levels of RSRQ compared to the original frequency of 3690 MHz: an increase from -14 dB to -11 dB. Moreover, S4 now exhibits comparable RSRQ performance to the neighboring PCI 150 of BS1, which is free of ACI. As compared with S3, the median throughput of S4 increased by approximately 12 Mbps, from 9 Mbps to 21 Mbps, while the peak throughput remained unchanged, as shown in Fig. 13(b).

A similar scenario is expected to occur between the 3.45 GHz and CBRS as 5G deployments in the $3.45-3.55$ GHz band increase (AT&T in U.S.), leading to further performance degradation for CBSDs operating at the lower edge of the CBRS band. Therefore, CBRS deployments must be aware of whether 5G is being deployed in the adjacent upper or lower bands to avoid using the band-edge CBRS channels, which are the most susceptible to ACI. Since the

TABLE III: Frequencies used by Verizon in the vicinity of the South Bend CBRS deployment.

Band	Freq. (MHz)	Band	Freq. (MHz)
CBRS, Band 48	3560, 3570, 3580, 3590, 3600, 3610, 3610, 3620, 3630, 3640, 3650, 3660, 3670, 3680	C-band, Bands n77/n78	3730, 3809

SAS does not provide this information, this intelligence must be obtained at the deployment site using measurement tools, such as those employed in this study, inspiring the development of more effective dynamic frequency allocation [19].

Although we recognize that focusing on a single deployment might appear limiting, the real-world deployment analyzed is substantial in size (4 locations and 18 PCIs spanning 12 km^2) and offers a rich, representative environment for studying the dynamics of channel allocation in the CBRS band with adjacent channels. Given its scale and variety, this deployment presents a valuable setting for understanding real-world challenges and yields insights that are applicable to other large-scale deployments [20]. There is no specific deployment pattern in South Bend: we believe that such deployments will exist elsewhere. Hence, as CBRS and 5G deployments (Verizon and AT&T) continue to expand, we believe that the findings from this measurement campaign can offer a solid foundation for broader discussions and future advancements for better CBRS band sharing, and do not represent a specific deployment pattern in South Bend.

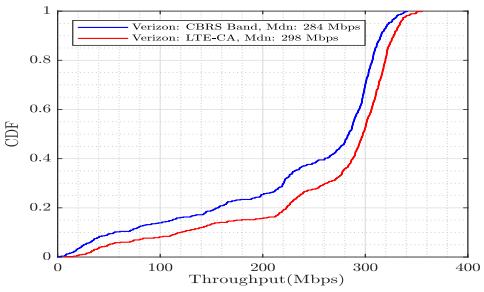

(a) CBRS and LTE-CA throughput.

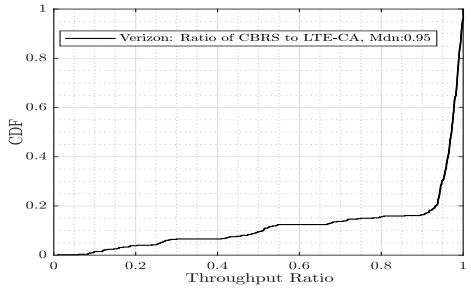

(b) Ratio of CBRS to total LTE-CA throughput.

Fig. 14: Verizon throughput with LTE-CA using CBRS.

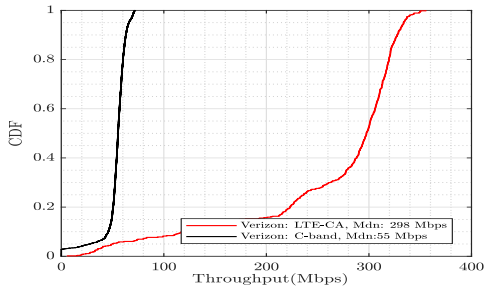

Fig. 15: Verizon LTE-CA and C-band throughput.

D. CBRS band use by Verizon using LTE-CA

During our experiments for MC-3, we observed that the Verizon BS also transmits on the CBRS band using LTE with CA (LTE-CA), aggregating up to five 20 MHz CBRS channels with four channels being aggregated most often (80%). Along with a 20 MHz primary LTE channel, this allows up to 120 MHz of bandwidth for use when high capacity is required: this is significantly higher than the C-band channel bandwidth of 60 MHz that Verizon has exclusive license for, but at a fraction of the cost compared to the billions spent on exclusive licenses. Table III details how the CBRS band (also referred to as Band 48), is utilized by Verizon in the vicinity of the South Bend CBRS deployment. We see that Verizon CBSDs are deployed on all available CBRS frequencies, creating potential CCI for other CBRS deployments. Interestingly, we observe that when Verizon uses LTE-CA combined with CBRS channels, both the total LTE-CA throughput and the proportion of throughput carried over the CBRS band are notably high, as illustrated in Fig. 14(a). The median throughput ratio of CBRS throughput and LTE-CA throughput is 0.95, as in Fig. 14(b), when at least one of the aggregated channels is a CBRS channel. Additionally, we sought to examine the throughput ratio between LTE-CA and the C-band. The overall throughput of Verizon 4G using LTE-CA was significantly higher than Verizon 5G using C-band at the same location, as shown in Fig. 15. This demonstrates that even as operators roll out 5G using their newly licensed spectrum, CBRS remains a highly competitive option when additional capacity is required.

IV. Propagation Modeling and Discussions

This section presents an analysis on use of existing empirical propagation models applicable to the CBRS band. The analysis utilizes measured RSRP data, collected through UEs, to derive the user-experienced propagation loss, as illustrated in Fig. 16. A comparison is then made between the user-experienced propagation loss and the path loss predicted by empirical models, with particular emphasis on the ITM as specified by CBRS standards.

A. Calculating user-experienced path loss

RSRP, as defined by the 3GPP, is the linear average over the power contributions (in watts) of the resource elements that carry cell-specific reference signals within the considered measurement frequency bandwidth [21]. In simpler terms,

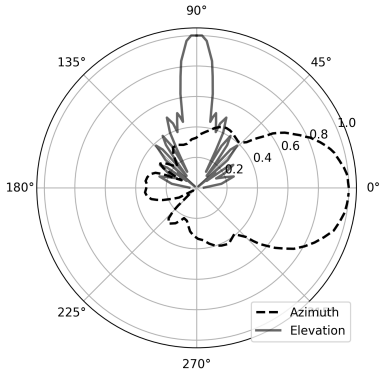

(a) Tx antenna directivity pattern $G_{Tx}(\theta, \phi)$.

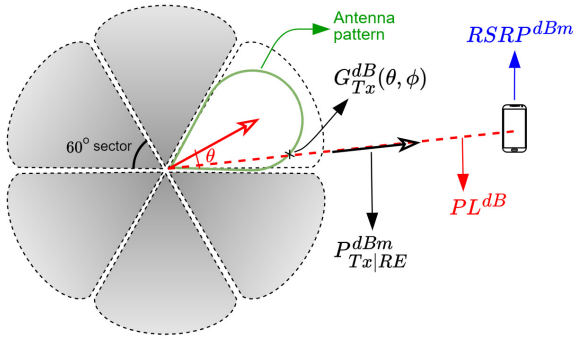

(b) Usage of antenna directivity pattern in analysis

Fig. 16: Tx antenna directivity pattern and its application in the propagation analysis.

RSRP represents the signal power received by the UE from the serving CBSD. This power depends on the conducted transmit power ($P_{Tx,C}$), the number of resource elements (N_{RE}), the antenna directivity gain ($G_{Tx}(\theta, \phi)$, with $\theta \in [0, 2\pi]$ and $\phi \in [0, \pi]$ representing the azimuth and elevation orientation of the UE relative to the CBSD), and the loss incurred in the propagation environment. The CBSDs deployed by city of South Bend uses a $P_{Tx,C}$ of 30 dBm/10 MHz for the allocated 20 MHz channel bandwidth (B) assigned to its network users. Assuming a subcarrier spacing (Δf) of 15 kHz typical in LTE networks, there are $N_{RE} = B/\Delta f$ resource elements over which $P_{Tx,C}$ is distributed for one symbol duration. The maximum allowable conducted power per RE ($P_{Tx,C|RE}$) for reference signaling purposes is determined as follows

$$P_{Tx,C|RE} = P_{Tx,C} - 10log_{10}(N_{RE}). \quad (1)$$

In addition to $P_{Tx,C|RE}$, antenna directivity gain is another critical factor influencing the propagation characteristics. Fig. 16(a) illustrates the normalized antenna directivity pattern of the AW3170 antenna used in this deployment [22]. A maximum antenna directivity gain of $\max\{G_{Tx}(\theta, \phi)\} = 17$ dBi is used, which complies with the FCC regulations, allowing up to 47 dBm/10 MHz EIRP [23] in outdoor CBRS deployment. Combining $P_{Tx,C|RE}$ with $G_{Tx}(\theta, \phi)$ results in the following mathematical model that describes the relationship between the calculated RSRP at the UE and the user-experienced

TABLE IV: Configuration parameters used by models.

PL Model	System parameters	Derived parameters	Variant-based tuning
3GPP UMa	f, d, h_{BS}, h_{UE}	Breakpoint distance	PL exponent PL intercept PL frequency dependence
ITU	f, d, h_{UE} Street width Representative clutter height	Single knife-edge diffraction loss Clutter loss	Clutter type
Winner-II	f, d, h_{BS}, h_{UE}	Breakpoint distance	PL exponent PL intercept PL frequency dependence
ITM	f, d, h_{BS}, h_{UE}	Terrain irregularity parameter Surface refractivity Earth's effective curvature Ground's surface transfer impedance	Climate type

propagation loss (PL), given as

$$RSRP = \underbrace{P_{Tx,C|RE} + G_{Tx}(\theta,\phi)}_{P_{Tx|UE}\text{: Power directed towards UE}} - PL. \tag{2}$$

This relationship is also illustrated in Fig. 16(b). On the UE side, the receive antenna pattern is proprietary and unavailable for analysis. A zero-gain receive antenna assumption is made, which is reasonable given that receivers are typically designed with low directivity to achieve omnidirectional characteristics and are optimized for low power consumption.

B. Empirical path loss models used

The following empirical path loss models are employed, with their system configuration parameters used as inputs, and summarized in Table IV.

3GPP 38.901 UMa model: The 3GPP 38.901 UMa (3GPP-UMa) propagation model is designed to account for potential exposure to LoS and NLoS characteristics of the environment across a broad frequency range, from 0.5 GHz to 100 GHz, and includes an alternative NLoS optional scenario [24].

ITU's Height gain terminal correction model: ITU propagation model on the other hand classifies its variants based on clutter profiling, grouping environments into rural, suburban, and urban categories [25].

Winner II model: The Winner II model adopts a comprehensive approach, associating each geographical category including rural, suburban, and urban with its respective LoS and NLoS options [26].

ITM-based CBRS model: The ITM does not account for geographical categories or LoS/NLoS distinctions. Instead, it focuses on the terrain profile to derive a terrain irregularity parameter and operates over a broad frequency range from 40 MHz to 100 GHz, with its variants based on radio climate types such as equatorial, continental subtropical, maritime, and others [13]. For our analysis, we fix the climate type to continental-subtropical, which is the predominant climate in the USA.

The CBRS standards specify the use of the ITM. In the initial release of the CBRS 1.0 standard, ITM was employed without any additional modifications. However, in the CBRS 1+ specification, the following two additional losses are added on top of ITM defined in CBRS 1.0 [27]:

1) For CBSDs with $h_{BS} < 6$ m, the following clutter loss (L_{ctt}) derived from ITU model [25] is added, as

$$L_{ctt} = \begin{cases} 0 & d < 0.25 \\ -5\log_{10}\left(10^{-6.1024} + \frac{10^{-6.9298}}{d^{4.78}}\right), & 0.25 \le d \le 2 \\ 30.5 & d > 2 \end{cases} \tag{3}$$

where L_{ctt} is in dB, and d in km.

2) An additional arbitrary loss of 8 dB is added to all CBRS 1+ specified ITM, accounting for TDD and network loading factors.

Elaborating on Table IV, the parameters f, d, h_{BS} and h_{UE} represent the following: f denotes the center frequency of the band assigned to the CBSD, d indicates the distance between the UE and the CBSD, h_{BS} refers to the height of the BS and h_{UE} represents the height of the UE, which is assumed to be the default value used by the models, typically set at 1.5 m. The calculation of d using the Haversine formula, based on the latitude and longitude coordinates of the measurement locations and their corresponding serving CBSD, is given by the following equation, as

$$d = 2r\arcsin\Bigg\{\Bigg(\sin^2\left(\frac{\alpha_2-\alpha_1}{2}\right) + \cos(\alpha_2)\cos(\alpha_1)\sin^2\left(\frac{\beta_2-\beta_1}{2}\right)\Bigg)^{1/2}\Bigg\}, \tag{4}$$

where r is the radius of the Earth (at the city of South Bend), and (α_1, β_1) and (α_2, β_2) represent the latitude and longitude coordinates of the BS and the measurement location, respectively, with all coordinates expressed in radians.

Given the diversity in model characteristics and applicability, an investigation of model fit is performed for each CBSD individually, employing the Root Mean Square Error (RMSE) parameter to evaluate the quality of fit, as

$$RMSE = \sqrt{\sum_{i=0}^{N-1} \frac{\left[PL_i - \widehat{PL_i}\right]^2}{N}}, \tag{5}$$

where PL_i represents the user-experienced path loss derived from measured data using Eq. 2. $\widehat{PL_i}$ denotes the predicted path loss at the corresponding measurement point based on a given empirical model, and N is the number of measured data points.

Evaluation is conducted to compare these propagation models, including the CBRS 1+ specified ITM, to determine which best represents the UE experienced path loss. The goal is not to achieve a close fit of the models to the data, but rather to analyze whether the models provide reliable predictions in non-ideal and practical measurement setups. This comparison is crucial for assessing the models' effectiveness in a real-world CBRS deployment, where ideal assumptions may not hold, and ensuring that the predictions are robust for practical deployment scenarios.

TABLE V: RMSE results for the best-fit model & ITM

BS	PCI	Best-fit		ITM	Proposed
		Model	RMSE	RMSE	RMSE
BS-1 $h_{BS} = 21, 29$ m	189	itu_urban	10.24	22.82	17.52
	150	3gpp-uma_nlos_optional	11.70	19.87	18.90
	194	3gpp-uma_nlos_optional	6.79	25.22	8.00
	6	3gpp-uma_nlos_optional	5.56	21.38	11.51
	169	3gpp-uma_nlos_optional	6.55	20.99	10.07
	195	itu_urban	6.08	17.67	14.59
BS-2 $h_{BS} = 44$ m	69	3gpp-uma_nlos_optional	6.61	17.47	11.66
	10	**itu_rural**	8.38	**8.70**	**22.78**
	78	win-ii_rural_nlos	8.57	16.34	17.03
	200	win-ii_rural_nlos	7.76	15.78	17.74
	1	win-ii_rural_nlos	9.23	15.06	20.89
	165	**win-ii_urban_los**	8.04	**10.04**	**24.49**
BS-3 $h_{BS} = 33$ m	88	win-ii_rural_nlos	8.73	17.50	16.35
	26	win-ii_rural_nlos	7.76	17.74	15.69
	14	3gpp-uma_nlos_optional	6.44	21.49	12.12
	96	3gpp-uma_nlos_optional	7.08	20.66	14.1
BS-4 $h_{BS} = 12$ m	187	win-ii_suburban_nlos	8.46	27.52	12.16
	46	3gpp-uma_nlos_optional	10.05	24.20	12.48

C. Results and Discussions

In the following, we present the results of the empirical propagation models listed in Table IV and compare them with real-world CBRS measurements under different scenarios.

Discussion for NLoS environment: The RMSE between the measured RSRP values for each PCI has been compared against thirteen different variants of propagation models outlined in Table IV, with the results shown in Table V. Among the contenders, the variants of the 3GPP-UMa propagation model emerge most frequently as the best-fit models, consistently appearing as the top choice for each PCIs. These models have been specifically developed for NLoS environments and demonstrate satisfactory performance, with RMSE values ranging from 5.56 dBm to 11.70 dBm, and a mean RMSE of 7.59 dBm. Also, the 3GPP-UMa best-fit models are mainly observed around BS-1, BS-3, and BS-4, which have lower antenna heights compared to the tallest BS (BS-2) and are situated in areas with dense foliage, leading to a higher likelihood of NLoS propagation. In addition, the NLoS variant of the Winner-II model appears as the second most frequent best-fit model in three out of the four BSs (BS-2, BS-3, and BS-4), with RMSE values ranging from 7.76 dBm to 9.23 dBm and a mean of RMSE 8.42 dBm. The best-fit models for RSRP values of PCI 189 and PCI 195 at BS-1, characterized by good throughput as shown in Fig. 5(a), are observed for the urban ITU model. This agrees with the presence of a dense environment, reflecting and obstructing the propagation signal, in the vicinity of BS-1. Unfortunately, the CBRS 1+ specified ITM performs poorly compared to the NLoS best-fit models, with RMSE values ranging from 15.06 dBm to 27.52 dBm and a mean RMSE of 20.11 dBm. Hence, improvement is needed on the performance of the CBRS 1+ specified ITM model for environments with dense foliage, dominant NLoS propagation and low antenna height.

Discussion for LoS environment: Among all PCIs, only PCI 165 and PCI 10 at BS-2 are characterized by LoS-based best-fit models, with PCI 165 associated with Winner-II model's rural LoS variant, and PCI 10 linked to the ITU model's rural variant. This outcome aligns with the environmental conditions observed during the measurement campaigns. The presence of LoS also agrees with PCI 165 achieving the highest median throughput (66 Mbps) in the CBRS deployment. It can also be observed that the best RMSE performance for the CBRS 1+ specified ITM occurs with PCI 165 and PCI 10, both operating in a dominant LoS environment. In fact, for these PCIs, the CBRS 1+ specified ITM shows RMSE performance comparable to that of the best-fit models, unlike its performance for other PCIs.

Discussion for CBRS 1+ specified ITM: As discussed above, the CBRS 1+ specified ITM performs well in LoS areas but struggles in NLoS areas. The model's poor performance in NLoS scenarios may be attributed to its limitations in effectively capturing the effects of clutter that obstructs LoS propagation. A further explanation lies in considering Eq. 3, where L_{ctt} is ignored due to the deployment having $h_{BS} >$ 6 m. This omission could explain why the CBRS 1+ specified ITM fails to account for clutter loss in such scenarios. This was further verified by a "**proposed**" model that removed the h_{BS} constraint, resulting in improved performance for NLoS dominant PCIs, but reduced performance for LoS dominant PCI 10 and 165.

These observations are also illustrated in Fig. 17. PCI 165 of BS-2 (the BS with the highest height) is chosen to demonstrate a LoS-dominant PCI and its performance, as shown in Fig. 17(a). Meanwhile, Fig. 17(b) shows PCI 46 of BS-4 (the BS with the lowest height), which does not experience any CCI like other PCIs in BS-4, chosen to demonstrate a NLoS-dominant PCI. In Fig.17, a sharp breakpoint in the proposed model is observed, which results from assigning $L_{ctt} = 0$ dB for $d < 0.25$ km. From Fig. 17(a), it can

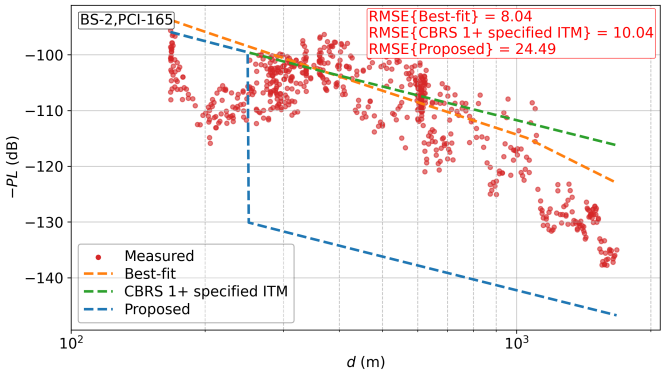

(a) LoS-dominant PCI 165

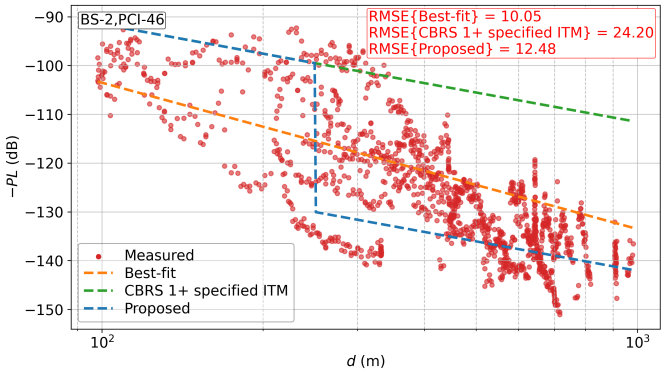

(b) NLoS-dominant PCI 46

Fig. 17: Path loss analysis performed on LoS-dominant PCI 165 and NLoS-dominant PCI 46.

be seen that the CBRS 1+ specified ITM model performs similarly to the best-fit model. However, with the introduction of L_{ctt} in the proposed model, excess loss is predicted, leading to an inaccurate representation of real-world conditions. In Fig. 17(b), best-fit model and CBRS 1+ specified ITM model perform differently, with best-fit model aligning more closely with measured data. However, introducing L_{ctt} through the proposed model brings the loss prediction closer to the measured data, and offers similar performance to the best-fit model for distances $d > 0.25$ km.

This leads to the following two conclusions: (i) L_{ctt} needs to be considered for $h_{BS} > 6$ m, and (ii) the environment should be categorized as LoS or NLoS dominant for accurate path loss prediction. Further analysis is required to refine the modeling of L_{ctt} for cases where $h_{BS} > 6$ m, as the performance of the proposed model, while improving NLoS predictions, does not fully align with the accuracy of best-fit models in many scenarios. This discrepancy suggests that simply removing the height constraint is insufficient to account for the complexities of clutter loss at greater BS heights. A more comprehensive approach is needed to incorporate the effects of clutter for taller deployments, ensuring that both LoS and NLoS scenarios are adequately addressed without compromising performance across different propagation conditions.

V. Conclusion

The extensive measurements and analyses presented in this study conclusively demonstrate that secondary coexistence among GAA CBSDs, even when they belong to the same CBRS network, can be a limiting factor for optimal performance. In the deployment we studied, all CBRS channels were available according to the Google SAS, however the South Bend CBRS deployment used three 20 MHz channels (3580 MHz, 3670 MHz and 3690 MHz) more often than the others. Further, the deployment did not take into account the emergence of Verizon CBRS using GAA mode in the vicinity, along with adjacent channel C-band, both of which further impacted the performance. In order to demonstrate the impact of appropriate frequency allocation, we worked with the CBRS provider to change the frequency of two CBSDs in different locations and demonstrated improved performance of signal quality metrics. However, this change took a while to implement since the SAS had to authorize the new channel. Thus, it is clear that CBRS deployments need to be able to dynamically change their operating channel based on measurements in the field: such dynamic behavior is not possible today since all channel allocations must be through the SAS provider. Further, we demonstrated that even with 4G, when multiple CBRS channels were aggregated, the throughput was higher than that obtained with 5G using C-band, thus demonstrating the usefulness of CBRS to both large mobile operators as well as small private network providers such as the South Bend school district. Future work will consider how channel choice by CBRS can be made more dynamic and other ways to better manage secondary coexistence among GAA users. Moreover, our propagation analysis indicates that more detailed and comprehensive clutter models need to be investigated, developed, and integrated into the existing CBRS specifications across different BS height constraints to improve the prediction performance of propagation loss for CBRS band.

Acknowledgment

This research was funded in part by NSF Grants AST-2132700, CNS-2346413 and CNS-2229387.

References

[1] S. A. A. Shah, E. Ahmed, M. Imran, and S. Zeadally, "5G for vehicular communications," *IEEE Communications Magazine*, vol. 56, no. 1, pp. 111–117, 2018.

[2] A. Ghosh and R. Berry, "Competition with three-tier spectrum access and spectrum monitoring," in *Proceedings of the 20th ACM International Symposium on Mobile Ad Hoc Networking and Computing*, 2019, pp. 241–250.

[3] The Wireless Innovation Forum. (2023) CBRS Operational Security. WINNF-TS-0071. [Online]. Available: https://cbrs.wirelessinnovation.org/release-1-standards-specifications

[4] P. Agarwal, M. Manekiya, T. Ahmad, A. Yadav, A. Kumar, M. Donelli, and S. T. Mishra, "A survey on citizens broadband radio service (CBRS)," *Electronics*, vol. 11, no. 23, p. 3985, 2022.

[5] W. L. Ross and S. D. W. Kinkoph, "Annual report on the status of spectrum repurposing," *Proceedings of the 2019, US Department of Commerce*, 2019.

[6] S. Dogan-Tusha, M. I. Rochman, A. Tusha, H. Nasiri, J. Helzerman, and M. Ghosh, "Evaluating the interference potential in 6 GHz: An extensive measurement campaign of a dense indoor Wi-Fi 6E network," in *Proceedings of the 17th ACM workshop on wireless network testbeds, experimental evaluation & characterization*, 2023, pp. 56–63.

[7] M. Paolini and S. Fili, "CBRS: Should the enterprise and venue owners care?" *Senza Fili*, 2019.
[8] C. W. Kim, J. Ryoo, and M. M. Buddhikot, "Design and implementation of an end-to-end architecture for 3.5 GHz shared spectrum," in *2015 IEEE International Symposium on Dynamic Spectrum Access Networks (DySPAN)*. IEEE, 2015, pp. 23–34.
[9] S. J. Maeng, O. Ozdemir, İ. Güvenç, M. L. Sichitiu, M. Mushi, R. Dutta, and M. Ghosh, "SDR-based 5G NR C-band i/q monitoring and surveillance in urban area using a helikite," in *2023 IEEE International Conference on Industrial Technology (ICIT)*. IEEE, 2023, pp. 1–6.
[10] Verizon. (2023) The map of approximate outdoor coverage of 5G Ultra Wideband for Verizon in USA. [Online]. Available: https://www.verizon.com/coverage-map/
[11] M. I. Rochman, V. Sathya, B. Payne, M. Yavuz, and M. Ghosh, "A measurement study of the impact of adjacent channel interference between c-band and cbrs," in *2023 IEEE 34th Annual International Symposium on Personal, Indoor and Mobile Radio Communications (PIMRC)*. IEEE, 2023, pp. 1–7.
[12] Z. Nadir and M. I. Ahmad, "Pathloss determination using Okumura-Hata model and cubic regression for missing data for Oman," in *Proceedings of the International MultiConference of Engineers and Computer Scientists*, vol. 2, 2010, pp. 17–19.
[13] G. Hufford, A. Longley, and W. Kissick, "A guide to the use of the its irregular terrain model in the area prediction mode," NTIA, U.S. Department of Commerce, Tech. Rep. NTIA Report 82-100, 1982.
[14] Federal Communications Commission, "Notice of proposed rulemaking, fcc-24-86a1," 2024. [Online]. Available: https://docs.fcc.gov/public/attachments/FCC-24-86A1.pdf
[15] A. Tusha, S. Dogan-Tusha, H. Nasiri, M. I. Rochman, P. McGuire, and M. Ghosh, "A comprehensive analysis of secondary coexistence in a real-world cbrs deployment," in *2024 IEEE International Symposium on Dynamic Spectrum Access Networks (DySPAN)*. IEEE, 2024, pp. 79–87.
[16] V. Sathya, M. I. Rochman, and M. Ghosh, "Measurement-based coexistence studies of LAA & Wi-Fi deployments in Chicago," *IEEE Wireless Communications*, vol. 28, no. 1, pp. 136–143, 2021.
[17] Rohde & Schwarz. (2023) QualiPoc: Handheld mobile network testing and trouble shooting. [Online]. Available: https://www.rohde-schwarz.com/us/products/test-and-measurement/network-data-collection/qualipoc-android_63493-55430.html
[18] EPiQ Solutions. (2023) PRiSM: Handheld network scanner and spectrum analyzer. [Online]. Available: https://epiqsolutions.com/rf-sensing/prism/
[19] M. Ghosh, A. Tusha, M. I. Rochman, J. R. Palathinkal, P. Krishnamurthy, and I. Murtazashvili, "Comments on FCC's NPRM on CBRS, Docket 17-258," Nov. 2024. [Online]. Available: https://www.fcc.gov/ecfs/document/1106214582907/1
[20] M. I. Rochman, W. Ye, Z.-L. Zhang, and M. Ghosh, "A comprehensive real-world evaluation of 5G improvements over 4G in low-and mid-bands," in *2024 IEEE International Symposium on Dynamic Spectrum Access Networks (DySPAN)*. IEEE, 2024, pp. 257–266.
[21] "LTE; Evolved Universal Terrestrial Radio Access (E-UTRA); Physical layer; Measurements (3GPP TS 36.214)," European Telecommunications Standards Institute, Tech. Rep. V12.2.0 Release 12, 2014.
[22] Alpha Wireless, "Alpha wireless AW3170 panel antenna fixed datasheet," 2023.
[23] "Requirements for commercial operation in the U.S. 3550-3700 MHz Citizens Broadband Radio Service Band," Wireless Innovation Forum, Tech. Rep. WINNF-TS-0112, 2020.
[24] 3GPP, "Technical Report; Study on channel model for frequencies from 0.5 to 100 GHz (Release 16)," 3GPP, Tech. Rep., Jul. 2020.
[25] "Recommendation ITU-R P.2108-1: Prediction of clutter loss," International Telecommunication Union, Tech. Rep., 2021.
[26] P. Kyosti and et. al., "WINNER II channel models D1.1.2 v1.2 final report," IST-4-027756 WINNER II, Tech. Rep., 2007.
[27] "Post initial certification revisions to CBRS baseline operational and functional requirements specification," Wireless Innovation Forum, Tech. Rep. WINNF-TS-1020, 2024.

Armed Tusha received his B.Sc. degree in Electrical and Electronics Engineering from Istanbul Sehir University, Istanbul, Turkey, in 2016. In August 2016, he joined the Communications, Signal Processing, and Networking Center (CoSiNC) at Istanbul Medipol University, Istanbul, Turkey, where he completed his M.Sc. degree in 2018 and his Ph.D. degree in 2023 in Electrical Electronics Engineering and Cyber Systems. He is currently a Postdoctoral Researcher at the University of Notre Dame, IN, USA. His current research interests are waveform design, signal processing, multicarrier schemes, orthogonal and non-orthogonal multiple accessing (OMA/NOMA) in wireless networks, index modulation, and channel coding, as well as wireless broadband measurements and mapping, and coexistence and interference management.

Seda Doğan-Tusha (Member IEEE) received the B.Sc. degree in Electronics and Telecommunication Engineering from Kocaeli University, Kocaeli, Turkey, in 2015, and the Ph.D. degree in Electrical and Electronics Engineering from Istanbul Medipol University, Istanbul, Turkey, in 2020. She is a Postdoctoral Researcher at the University of Notre Dame, IN, USA. Her research interests include orthogonal time frequency space (OTFS) modulation, index modulation (IM), millimeter-wave frequency bands, non-orthogonal multiple accessing (NOMA), channel control mechanisms, spectrum sharing, and coexistence techniques for next-generation wireless networks.

Joshua Roy Palathinkal (Graduate Student Member, IEEE) received the B.Tech. degree in Electronics and Telecommunication Engineering from the Indian Institute of Engineering Science and Technology, Shibpur, India, in 2021, and the M.S. degree in Electrical Engineering from Drexel University, PA, USA, in 2023. He is currently pursuing the Ph.D. degree in Electrical Engineering and an M.S. degree in Applied and Computational Mathematics and Statistics at the University of Notre Dame, Notre Dame, IN, USA. His research interests include wireless communication systems, dynamic spectrum sharing, coexistence strategies, and signal processing. He is a recipient of the 2022 Circuits, Systems, and Signal Processing Best Paper Award and multiple graduate fellowships.

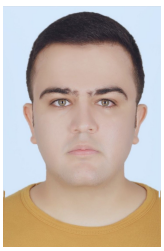

Hossein Nasiri is a third-year Ph.D. student in the Department of Electrical Engineering at the University of Notre Dame, IN, USA. He earned his B.Sc. degree from Shiraz University, Shiraz, Iran, in 2015 and his M.Sc. degree from Sharif University of Technology, Tehran, Iran, in 2019, both in Electrical Engineering. His research interests include machine learning and its applications in optimizing spectrum sharing.

This article has been accepted for publication in IEEE Transactions on Cognitive Communications and Networking. This is the author's version which has not been fully edited and content may change prior to final publication. Citation information: DOI 10.1109/TCCN.2025.3567608

Muhammad Iqbal Rochman received the Ph.D. degree in Computer Science from the University of Chicago. He is currently a Postdoctoral Researcher with the University of Notre Dame, where he investigates the real-world performance of cutting-edge radio technologies like Wi-Fi 7 and 5G, utilizing commercial off-the-shelf devices such as smartphones and single board computers to confirm analytical and lab-controlled measurements. The measurement data derived from this work enables his research in the critical area of spectrum sharing, specifically within the 6 GHz band and the proposed lower 3 GHz and 7 GHz bands.

Patrick McGuire received the B.A. degree in Economics and Sociology from the University of Notre Dame, South Bend, IN, USA, in 2021. He is currently the Director of Civic Innovation for the City of South Bend, IN, USA. In this role, Patrick works with community and research partners on novel and grant-funded initiatives serving South Bend residents across digital equity, smart city, and transportation portfolios. Prior to working for the City, he was an Innovation Fellow and Project Manager for the civic innovation nonprofit enFocus.

Monisha Ghosh is a Professor of Electrical Engineering at the University of Notre Dame. She is also the Policy Outreach Director for SpectrumX, the first NSF Center for Spectrum Innovation and the co-chair of the FCC's Technological Advisory Council (TAC) Working Group on Advanced Spectrum Sharing. Her research interests are in the development of next-generation wireless systems: cellular, Wi-Fi and IoT, with an emphasis on spectrum sharing and coexistence. Prior to joining the University of Notre Dame in 2022, she was the Chief Technology Officer at the Federal Communications Commission, a Program Director at the National Science Foundation, Research Professor at the University of Chicago and spent 24 years in industry research at Bell Labs, Philips Research and Interdigital working on a wide variety of wireless systems: HDTV, Wi-Fi, TV White Spaces and cellular. She obtained her BTech from IIT Kharagpur in 1986 and PhD from USC in 1991. She is a Fellow of the IEEE.